CHAPTER 3

Green synthesis of fluorescent carbon quantum dots from *Azadirachta indica* leaves and their peroxidase-mimetic activity for the detection of H_2O_2 and ascorbic acid in common fresh fruits

3.1. Introduction

Natural enzymes have been broadly used in various fields such as medicine, agriculture, industry and foods due to its high specificity and catalytic efficiency [Dong *et.al*. (2012)]. Peroxidase is a natural enzyme which catalyzes H_2O_2-dependent oxidoreduction and converts chromogenic substrates into a colored product. Therefore, peroxidases have been widely applied to biochemical analyses [Ryan *et.al*. (2006)]. The chromogenic substrate TMB has been widely used as a peroxidase substrate because of its high precision and sensitivity towards peroxidase based detection [Wang *et.al*. (2014)]. However, due to the rigorous storage condition, short storage life, high cost, and poor thermal stability limits their potential applications [Chen *et.al*. (2014)]. Therefore, enormous attention has been devoted towards the production and discovery of nanomaterials which can acts as a peroxidase-like activity. Firstly in 2007, Gao et al. were discovered Fe_3O_4 magnetic nanoparticles exhibited an intrinsic peroxidase-like enzyme activity [Gao *et.al*. (2007)]. Afterwards, a variety of nanomaterials including metal oxides ($ZnFe_2O_4$, V_2O_5), [Su *et.al*. (2012), Qu *et.al*. (2014)], metal sulphides (MoS_2, CuS) [Yu *et.al*. (2018), He *et.al*. (2012)], noble metals (Au, Ag, Pd) [Drozd *et.al*. (2016), Wang *et.al*. (2014), Wei *et.al*. (2015)], quaternary CuZnFeS nanocrystals [Dalue *et.al*. (2015)], graphene oxide [Wang *et.al*. (2014)], metal-organic framework (MOFs) [Gao *et.al*. (2017), Zheng *et.al*. (2018)], iron doped $CuSn(OH)_6$ Microspheres [Liu *et.al*. (2018)], ternary Polyaniline−MnO_2−Pd Nanowires [Zhong *et.al*. (2018)] and nitrogen-doped carbon nanomaterials [Hu *et.al*. (2018)] were discovered that had peroxidase-like activity in association with H_2O_2. The important characteristics of these enzyme-mimetic nanomaterials were found to detect H_2O_2, glucose [Li *et.al*. (2018)], immune assay [Dong *et.al*. (2014)], glutathione [Li *et.al*. (2018)], and cancer cell detection. However,

one of the major limitation of these nanomaterials were their synthesis from doping of chemical materials and the use of expensive and toxic chemicals along with multistep synthesis made it tedious process which limits the application of these nanomaterials [Salam *et.al*. (2012)]. Contrary to this, the use of natural precursors is advantageous because they are renewable, biocompatible and can convert biomass waste into the worthy and valuable materials [Zhang *et.al*. (2018)]. Addition to this, the natural precursors are excellent substitute over hazardous chemicals towards the synthesis of carbon-based nanomaterials because of many advantages such as economical, nontoxic, and high abundance [Liu *et.al*. (2012), Mohammadinejad *et.al*. (2016)]. Recently, several literatures have been reported towards the synthesis of carbon based nanomaterials from the natural precursors such as orange juice [Sahu *et.al*. (2012)], green tea [Wei *et.al*. (20124], egg [Wang *et.al*. (2012)], potatoes [Shen *et.al*. (2017)], lotus root [Gu *et.al*. (2016)], pepper [Yin *et.al*. (2013)], and coriander leaves [Sachdev *et.al*. (2015)]. Although, their applications were different such as detection of metal (Fe^{+3}, Hg^{+2}), hypo chloride, anti-oxidants, cell-imaging etc.

Ascorbic acid (AA) is a natural reductant molecule which is highly water soluble and acts as a reducing agent in many of the oxidation-reduction processes in the living organism. The antioxidants properties of AA are helpful in cancer prevention and immunity development. Moreover, it also protects LDL cholesterol from the oxidative damage because it is important for the formation of collagen protein which strengthens the muscles and blood vessels. The deficiency of AA causes many problems including the common cold, mental illness, in-fertility, scurvy, cardiovascular diseases, Parkinson's diseases and cancer. Therefore, to monitor the quantity and diet guidance in clinical, pharmaceutical and the food industry, the sensing of AA

have gain more attention. Although, varieties of techniques have been employed for the AA detection [Elgailani *et.al*. (2017), Pardakhty *et.al*. (2016), Guclu *et.al*. (2005), Gocmen *et.al*. (2000)]. Yet these are highly expensive, time-taking, requirement of sophisticated instrument and trained operator. Recently X. Luo et al. have reported the AA detection in common fruits via non-ecofriendly chemical derived carbon dots [Luo *et.al*. (2018)]. Therefore, development of simple, cost-effective and green precursor based carbon quantum dot is urgent need to avoid these limitations.

Keeping these limitations herein, we have synthesized carbon quantum dots from the zero cost, nontoxic, economical viable green precursor i.e. leaves of *Azadirachta indica* (neem) by eco-friendly one pot hydrothermal method without passivation of any chemical materials (**Scheme 3.1**).

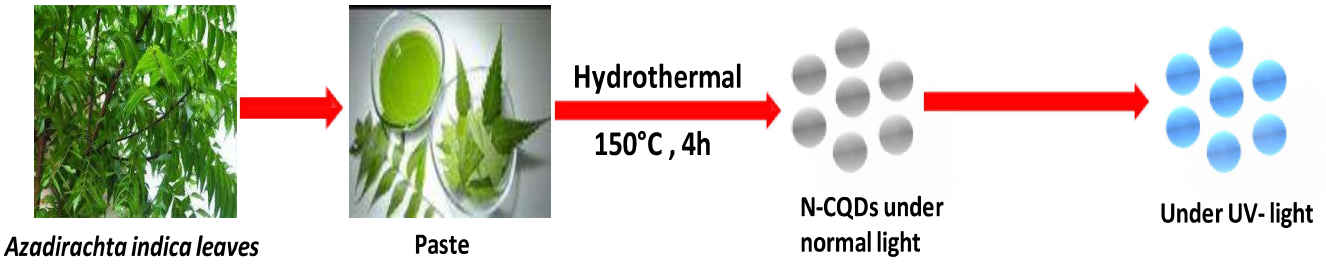

Scheme 3.1. The Synthetic methodology adopted for one pot hydrothermal synthesis of N-CQDs.

The medicinal properties of neem leaves are helpful to prevent many diseases. The main constituents are hydrocarbon, oxygen and nitrogen. The as-synthesized N-CQDs were well characterized through a variety of instrumentation techniques like TEM, P-XRD, FTIR, Zeta

potential and XPS. Although some literatures have been reported from *Azadirachta indica* having applications as antibacterial, antimicrobial, antifungal etc [Lalitha *et.al.* (2013), Roy *et.al.* (2017), Pandey *et.al.* (2013)]. However, a fluorescent CQDs having appreciable quantum yield and its application toward oxidation of TMB to show peroxidase-like activity has not been reported yet. Addition to this, the H_2O_2 dependent oxidation provides an efficient tool to detect H_2O_2 and AA in the real sample. These findings open a new channel for real-time investigation of ascorbic acid in complex biological system.

3.2. Experimental section

3.2.1. Chemicals and Materials

The *Azadirachta indica* leaves were obtained from nearby area of Vishwanath Temple, IIT (BHU), Varanasi, U.P., India. The other materials like hydrogen peroxide (H_2O_2), tetramethylbenzedine (TMB) and all reducing agents were purchased from the commercial supplier. The chromogenic substrate (TMB) was procured from Sigma Aldrich, India whereas H_2O_2 was purchased from Sd-fine chemicals limited, India. KBr, KI, glucose, benzoic acid, citric acid, ascorbic acid, etc. were purchased from Avra chemicals limited, India. The stock solution of all above mentioned reducing agents were prepared in distilled water. The fresh fruits were purchased from shops and all amino acid such as cystine (Cys), valine (Val), tryptophan (Trp), Alanine (Ala), aspartic acid (Asp), phenylalanine (Phe), serine (Ser), tyrosine (Tyr), threonine (Thr) and proline (Pro) were purchased from Avra chemicals limited, India. The whole experiments were performed in distilled water.

3.2.2. Hydrothermal Synthesis of Neem-Carbon quantum dots (N-CQDs)

Initially, 10 g fresh Neem leaves were crushed into the powder and dissolved in 100 mL of distilled water. Further, the suspension was poured into a 250 mL of Teflon-lined autoclave and kept in the oven at 150 °C for 4 hours. The autoclave was cooled naturally at room temperature (RT) after completion of reaction and obtained brown carbonaceous solution was centrifuged at 15000 rpm for 10 min to eliminate the larger particles. The supernatant of the centrifuged part were taken out and dialyzed for 24h in distilled water. Finally, a pure and clear brown color N-CQDs were obtained and kept at 4 °C for further use.

3.2.3. Apparatus and Characterization

The as-synthesized N-CQDs were characterized by the various instrumental techniques. The UV-visible absorption spectra were conducted by Thermo scientific EVOLUTION 201 spectrophotometer. The fluorescence emission spectra were recorded on Varian Cary Eclipse fluorescence spectrophotometer. The average size and morphology of the N-CQDs were confirmed by Transmission Electron Microscopy (TEM, TECHNAI 20 G2). Energy dispersive X-ray spectroscopy (EDAX) was obtained through the TEM analysis. The Powder X-ray diffraction (P-XRD) pattern was obtained on a Rigaku Smart lab. The Fourier-transform infrared spectrum (FTIR) was conducted on (Perkin Elmer Spectrum 100) in a range from 500 to 4000 cm^{-1}. Zeta potential was performed by Nano Zeta-Sizer Malvern apparatus. The elemental composition and surface state was determined by X-ray photo electron spectroscopy (XPS) (AMICUS, kratuos, Analytical, Ashimadzu) with Mg Kα excitation (1253.6 eV) radiation.

3.2.4. Quantum yield determination

The QY of the N-CQDs was calculated in reference to the quinine sulphate (QY = 54 % in 0.1 M H_2SO_4) at the excitation wavelength of 340 nm. The absorbance under 0.1 was noted at 340 nm and integrated emission intensity of quinine sulphate solution was also calculated at the excitation wavelength of 340 nm. The similar measurements were carried out for the N-CQDs with the same parameters, and the QY was measured as shown in **Table 3.1** using **Equation** mention in chapter 2 section 2.4. **1**.

Table 3.1 Calculation of fluorescence quantum yield with integrated intensity and absorbance of quinine sulphate and N-CQDs at excitation wavelength 340 nm.

Sample	Integrated intensity at 340 nm	Absorbance at 340 nm	Quantum yield (%)
Quinine sulphate (reference)	52513	0.056	54
N-CQDs	24521.10	0.052	27.2

3.2.5. Peroxidase-mimetic activity of N-CQDs

With the help of chromogenic substrate TMB and H_2O_2 the peroxidase-mimitic activity of N-CQDs was performed as follow: 40 µL of 1.2 mmol/L TMB + 35 µL of 0.7 mmol/L of H_2O_2 were mixed with 1 mL acetate buffer (0.2 M at pH 4). After that, 30 µL of N-CQDs (40 mg mL^{1}) was added in solution and UV- visible absorption spectra were traced with the color change of the solution.

The kinetic study was performed by keeping the concentration of one substrate fixed with changing the other and vice versa. In the first experiment fixed the concentration of TMB (0.8 mmol/L) and varied the H_2O_2 concentration (0.1 to 1 mmol/L). In the similar way fixed the

concentration of H_2O_2 (0.5 mmol/L) with varies the TMB concentration (0.2 to 1.2 mmol/L) and their UV-visible absorbance spectrum were performed on time course mode. The Lineweaver-Burk plot of TMB oxidation was used to determine the Km and Vmax parmeter of the reaction system.

3.2.6. Detection of hydrogen peroxide

The detection of H_2O_2 were conducted as follows: 40 µL of 8 mmol/L TMB + 30 µL N-CQDs (40 mg mL^{-1}) in 1.0 mL of 0.2 M NaAc buffer of pH 4.0, after that various concentration of H_2O_2 ranges from 0.02 to 2 mmol/L were added and kept for 10 minutes at the RT. Then UV-visible absorption spectrum was recorded and LOD was measured with the formula 3σ/s along with the S/N ratio 3, where 's' denoted slope of the linear curve and σ represent the standard deviation.

3.2.7. Detection of ascorbic acid

The detection of AA was performed as: 40 µL of 8 mmol/L TMB + 30 µL of N-CQDs (40 mg mL^{-1}) + 35 µL of 8 mmol/L H_2O_2 in 1 mL 0.2 M sodium acetate buffer (pH 4) along with incubation for 10 minutes at the RT to produced blue color of oxidized TMB. Afterward, the blue color solution was treated with different AA concentration ranging from 0 to 120 µM and UV-vis absorbance spectrum was recorded. Finally the LOD was calculated by using formula 3σ/s with the signal to noise ratio 3. Similarly, the interference test was carried out by replacing ascorbic acid with other reducing agents such as KBr, KI, glucose, cinnamic acid, benzoic acid, citric acid, oxalic acid, adipic acid, tartaric acid, uric acid and dopamine.

3.2.8. Detection of ascorbic acid in the real sample

The AA containing fruits were collected and the edible part of all the fruits were isolated and accurately weighed. Then the weighed sample was dissolved in 5 mL distilled water and centrifuged at 5000 rpm for 25 min in a refrigerated centrifuge at 5°C to remove the impurities. After that, the extract was filter through a 0.45 μm polyether sulfone (PES) membrane and equally diluted. Then, 1 mL of blue color ox-TMB solution was treated with 40 μL of different real sample from tomato to guava in a series and their UV-visible absorption spectra were recorded.

3.2.9. Investigation of hydroxyl radical

To determine the reactive species involved in the oxidation of TMB, hydroxyl radical (·OH) scavenger such as isopropyl alcohol (IPA) and methyl alcohol (MA) were added to the reaction medium and UV-visible absorbance spectrum was recorded.

3.3. Results and discussion

3.3.1. Characterizations

The size and morphology of the as-synthesized N-CQDs were explored through the high resolution TEM analysis. **Figure** 3.1**a** showed the spherical shape of N-CQDs while **Figure 3.1b** showed the corresponding histogram which confirmed that the average size of N-CQDs was 3.2 nm distributing in the narrow range from 1 to 5.5 nm. The broad ring in the selected area electron diffraction (SAED) pattern indicated the amorphous nature of the as-synthesized N-CQDs (**Inset Figure 3.2a**). The amorphous nature was further confirmed by P-XRD analysis with a broad peak at 2θ = 24.5° of carbonaceous materials (**Figure 3.1c)** [Deng *et.al*. (2017), Wang *et.al.* (2014)]. The energy dispersive X-ray analysis (EDAX) elaborated the presence of C (81.56 %),

O (9.82 %) and N (7.15 %) element present in a synthesized N-CQDs (**Figure 3.2**). However, the functional groups on the N-CQDs surface was confirmed by FT-IR spectroscopy with the band at 3411 cm^{-1}, attributed to the O–H stretching. The peaks at 2921cm^{-1} and 2853 cm^{-1} were due to the C-H stretching vibrations [Sun *et.al*. (2015). kovacova *et.al*. (2018)], while the band at 1736 cm^{-1} showed the presence of C=O stretching, the peak at 1654 cm^{-1} was associated with N-H bending. The band at 1457 cm^{-1} attributed to C=C whereas the peak at 1280 cm^{-1} indicated the C-O/C-N stretching (**Figure 3.1d**). These observations established the existence of the different functional group such as (-OH, -NH_2, and C=O) [Lin *et.al*. (2015)].

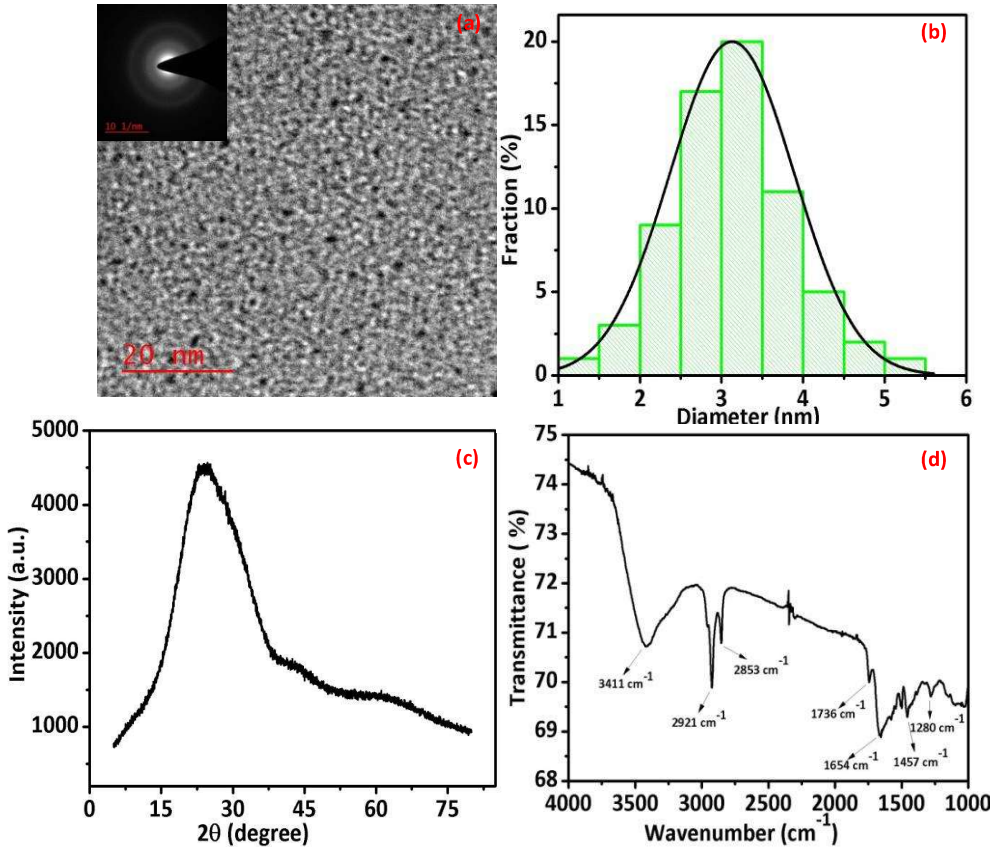

Figure 3.1 (a) High resolution TEM micro-image of the synthesized N-CQDs at 20 nm magnification, (b) size distribution graph, (c) P-XRD spectrum ranges between 5-80°, and (d) represents the FTIR spectrum of the N-CQDs.

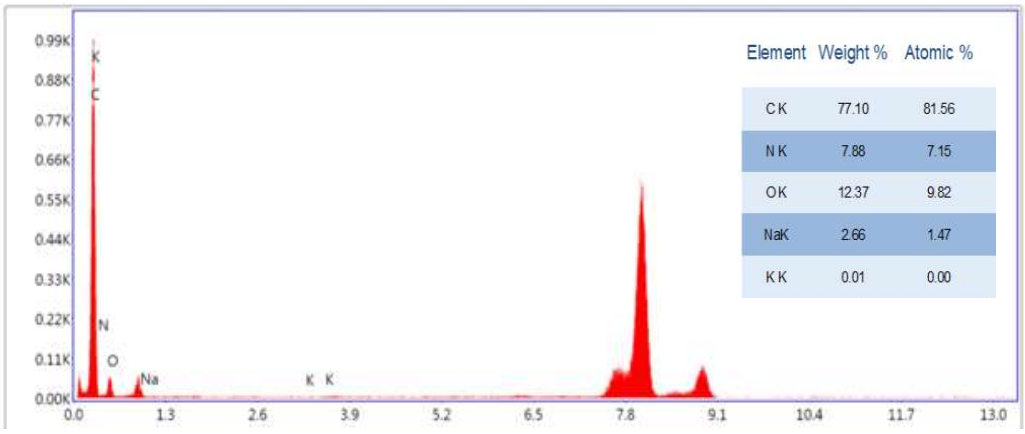

Figure 3.2 Energy dispersive X-ray analysis (EDAX) images of N-CQDs.

Further, the Zeta potential of the synthesized N-CQDs was -4.78 mV which showed the presence of negative charge on the N-CQDs surface (**Figure 3.3**).

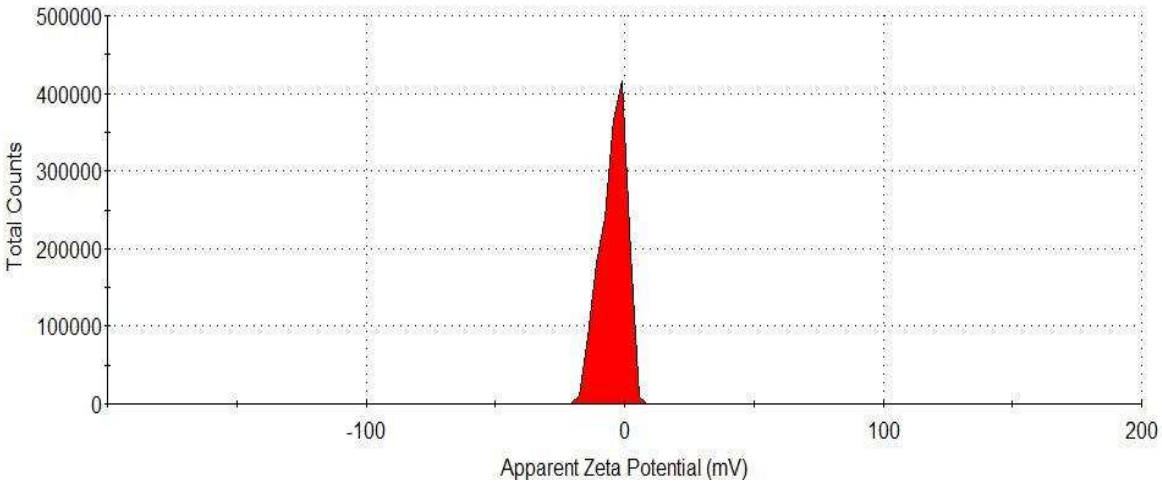

Figure 3.3 Zeta potential of the as-synthesized N-CQDs.

The different surface functional states and bond present on the synthesized N-CQDs were further probed through XPS investigation. The full scan XPS spectrum showed the characteristic peaks correspond to C 1s (285.70 eV), N 1s (400.59 eV) and O 1s (533.22 eV) which confirmed the presence of C, N, and O in their structure (**Figure 3.4a**). A close look of C 1s spectrum of the N-CQDs exhibited the four peaks located at 288.08, 284.79, 286.83 and 285.70 eV, ascribed the C=O, C=C/C-C, C-O and C-N groups correspondingly (**Figure 3.4b**) [Tang *et.al.* (2012), Huang *et.al.* (2014)]. The N 1s high-resolution XPS spectrum displayed three peaks at 401.80, 400.79, and 399.91 eV, corresponds to pyrrolic N, pyridinic N and C-N-C respectively (**Figure 3.4c**) [Hu *et.al.* (2018)]. The O 1s spectrum resolved into the three peaks at 531.95, 533.76 and 532.94 eV, may be due to the C-OH, N=O and C-O-C/C=O correspondingly as shown in **Figure 3.4d** [Kong *et.al.* (2018)]. All the experimental analysis were consisted through each other and showed successful preparation of N-CQDs.

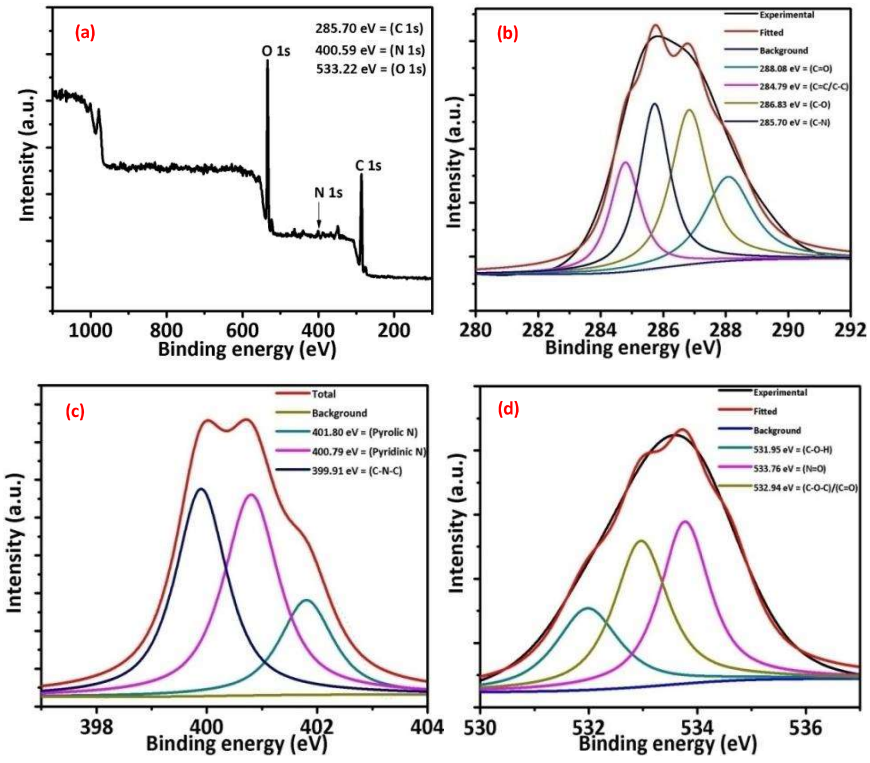

Figure 3.4 XPS survey (a) full scan (b) C 1s, (c) N 1s, and (d) O 1s spectrum of the as-synthesized N-CQDs.

3.3.2. Optical Studies

To evaluate the optical properties of synthesized N-CQDs, UV–Vis absorbance spectra were measured. The spectrum showed two absorption band at 276 nm and 340 nm which ascribed to the π–π* and n–π* transition correspondingly (**Figure 3.5**).

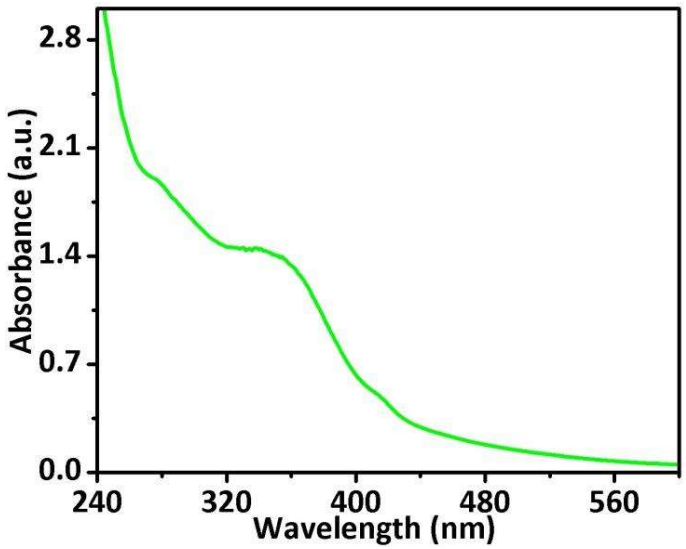

Figure 3.5 UV-visible absorbance spectrums of the N-CQDs.

To confirm, whether the N-CQDs show excitation dependent fluorescence emission or not, different fluorescence emission spectra on varying excitation wavelengths from 290 to 370 nm were traced. Initially, when the excitation increased up to 340 nm, the fluorescence emission intensity gradually increased with a red shift and the maximum fluorescence emission intensity

was obtained at 340 nm of excitation wavelength along with corresponding emission 467 nm. However, further change of the excitation wavelength from 350 nm to 370 nm, the emission intensity decreased gradually as shown in **Figure 3.6**. The QY of as-synthesized fluorescent N-CQDs was about 27.2 % in reference to quinine sulphate.

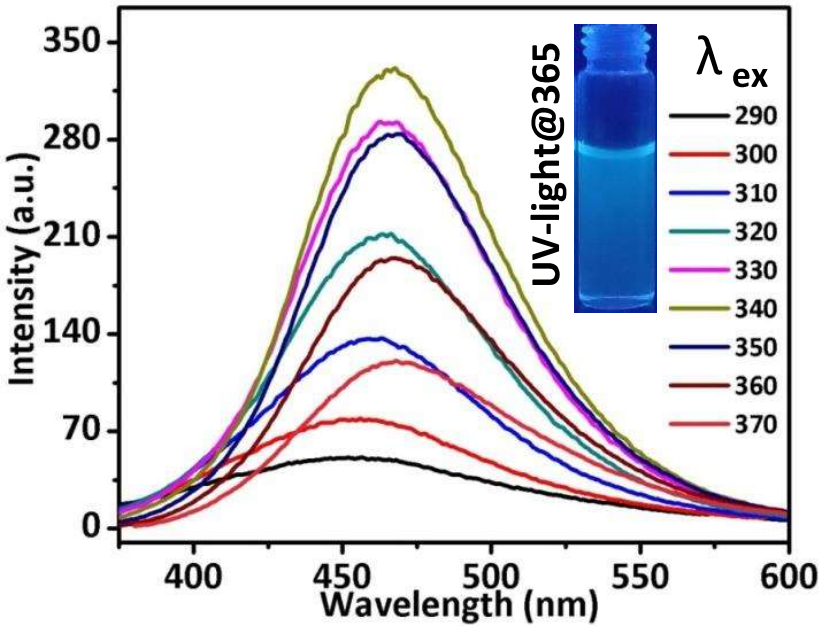

Figure 3.6 Represents the fluorescence emission spectra of the N-CQDs at the different excitation wavelength ranged from 290 nm to 370 nm with the difference of 10 nm.

The pH effect on the fluorescence emission of as-synthesized N-CQDs was also investigated. The **Figure 3.7** confirmed that changing the pH of solution has effect on the fluorescence intensity of the N-CQDs but no effect on emission wavelength. As the pH increased from 2 to 7, the emission intensity increased up to pH 7, meanwhile as the pH increased from 7

to 12, the fluorescence emission intensity decreased gradually. It was further supported by their blue fluorescence (**inset Figure 3.7**). This result indicated that as-synthesized N-CQDs can be mostly used in wide pH range 5 to 9.

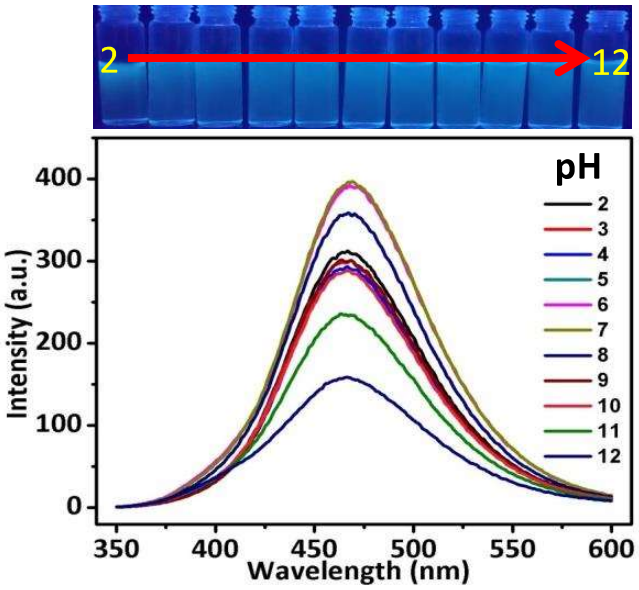

Figure 3.7 Study of pH change on the fluorescent intensity of N-CQDs with corresponding photograph under UV – light (λex = 365 nm) from pH range 2 to 12.

To further investigate the effect of ionic salt on the fluorescence emission intensity, the as-synthesized N-CQDs were treated with different KCl solution (0.5 to 5 M) and were observed that varying concentration of salt has no considerable effect on fluorescence emission intensity of N-CQDs (**Figure 3.8**).

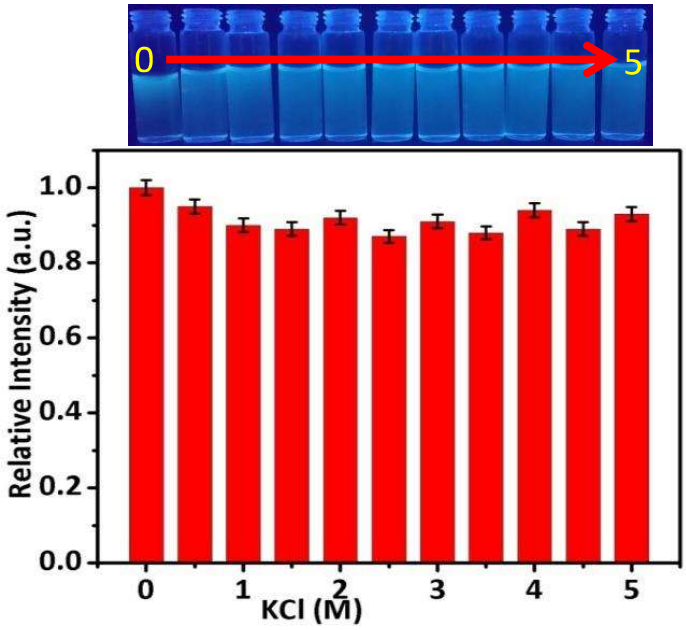

Figure 3.8 Effect of ionic strength on emission spectra of N-CQDs with photograph under UV- light (λex = 365 nm).

3.3.3. Peroxidase-mimetic activity of the synthesized N-CQDs

The catalytic activity of N-CQDs was performed as: first of all, UV–visible absorption spectra of (40 µL TMB + 30 µL N-CQDs in 1mL acetate buffer at pH 4) mixture were carried out which showed negligible absorbance at 652 nm (black line) without color change of the solution indicated that no oxidation of TMB occurred. Further, (40 µL TMB + 35 µL H_2O_2 in a 1 mL of NaAc buffer at pH 4) showed a less intense peak at 652 nm (red line) stated the partial oxidation of TMB with the appearance of partial blue color. However, in the existence of 30 µL N-CQDs (40 µL TMB + 35µL H_2O_2 in 1 ml acetate buffer) the absorbance was maximum at 652 nm and 365 nm (blue line) with the color change from colorless to the blue (**Figure 3.9**). These

observations strongly confirmed that N-CQDs showed peroxidase-like activity [Yang *et.al*. (2017)].

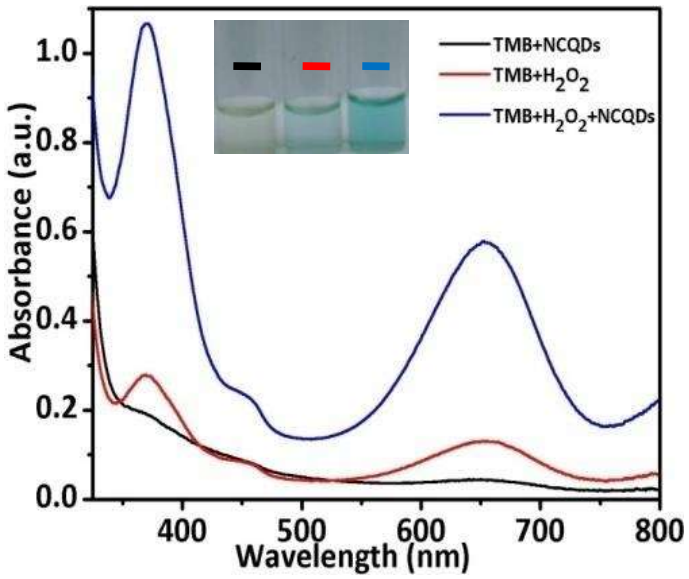

Figure 3.9 Represents the UV-visible absorption spectra of varies reaction system: TMB + N-CQDs, TMB + H_2O_2 and TMB + H_2O_2 + N-CQDs whereas inset photograph shows the corresponding color change.

Addition to this, the stability of peroxidase-like activity of N-CQDs was also investigated. To explore the long term stability, the as-synthesized N-CQDs were kept at a RT for several days and the catalytic activity was precisely measured over a three weeks. It can be seen from the **Figure 3.10** that only a small decrease in the catalytic activity, demonstrating that the N-CQDs have excellent long term stability over three-week.

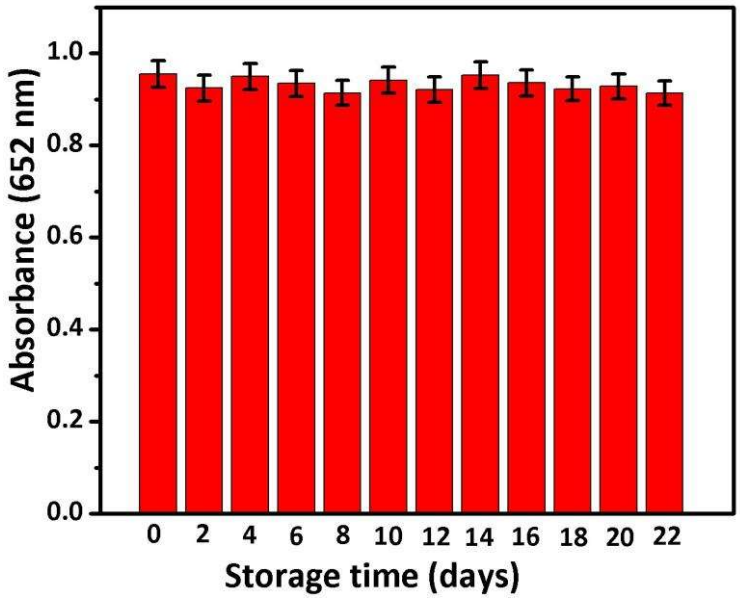

Figure 3.10 Long term stability experiment for the peroxidase-mimetic catalytic activity of N-CQDs.

3.3.4. Optimization of different experimental conditions

The catalytic activities are highly influence by the change in pH, temperature, course of reaction time and substrate concentration (H_2O_2 and TMB). Therefore the catalytic activity of N-CQDs also influences by these parameters during oxidation of TMB. To optimize these parameters such as pH and temperature, UV-visible absorption spectra were carried out at different pH from 2 to 6 and temperature from 10 to 50 °C. It can be seen from the **Figure 3.11a, b** and **Figure 3.12 a, b** the maximum absorption was occurred at pH 4 and temperature 35° of the oxidized TMB indicating the maximum catalytic activity of N-CQDs respectively. These

observations were further confirmed by the intensive blue color of ox-TMB (**Inset Figure 3.11a** and **b**). Similarly the absorption spectra of TMB oxidation at different concentration of H_2O_2 (1 to 10 mmol/L) was investigated and it was observed that maximum absorption occurred at 8 mmol/L of H_2O_2 (**Figure 3.11c** and **Figure 3.12c**) along with color change from transparent to blue (**Inset Figure 3.11c**). Similarly, the maximum absorption was occurred at 8 mmol/L of TMB after changing the concentration of TMB from 1 to 10 mmol/L (**Figure 3.11d** and **Figure 3.12d**). The course of reaction time was investigated by varying the incubation time (10 to 50 min), indicated maximum absorption at 35 min of reaction time (**Figure 3.11e** and **Figure 3.12e**) along with the formation of intense blue color (**Inset Figure 3.11e**). Thus, the maximum catalytic activity of as-synthesized N-CQDs was at pH 4, temperature 35°, H_2O_2 and TMB 8 mmol/L at 35 min of reaction time.

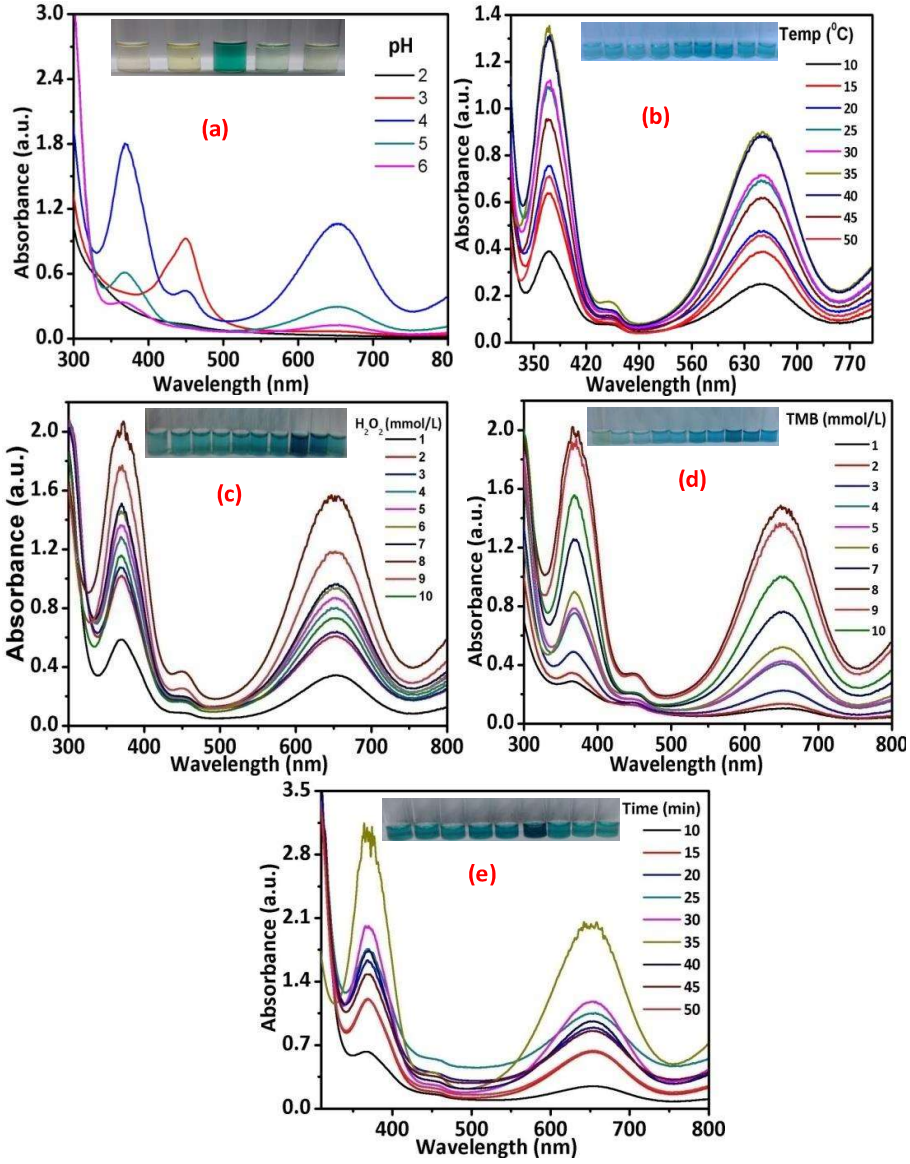

Figure 3.11 Represents the UV-visible absorption spectra towards peroxidase-mimetic activity of N-CQDs on varying (a) pH of the solution from 2 to 6, (b) temperature from 10 to 50°, (c) H_2O_2 concentration (1-10 mmol/L), (d) TMB concentration (1-10 mmol/L) and, (e) Time respectively where inset shows the corresponding color change at different reaction conditions.

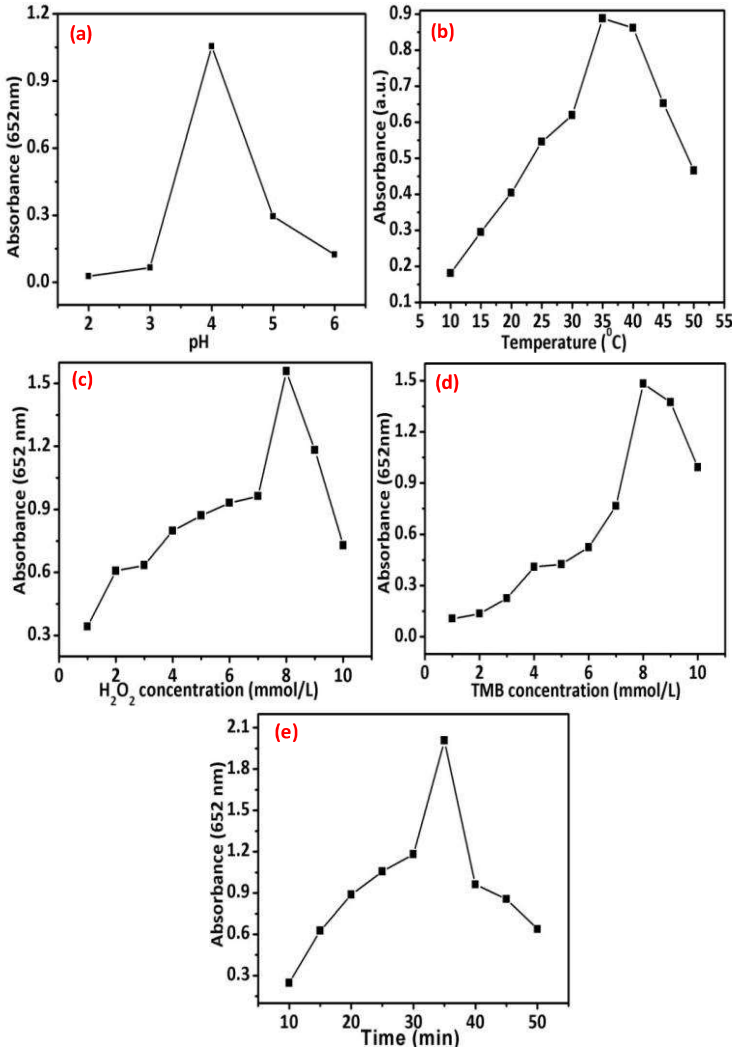

Figure 3.12 Dependence of relative activity of peroxidase-like catalytic reactions by N-CQDs on the (a) pH (b) temperature (c) H_2O_2 concentration, (d) TMB concentration and (e) Time.

3.4. Kinetic analysis

On changing the one substrate concentration keeping other substrate as fixed, the Michaelis-Menten kinetic parameters were investigated to establish the peroxidase-mimetic activity of N-

CQDs. The initial velocity was determined by time course mode, i.e. changes in absorption at 652 nm by changing the substrate concentrations with time. The found absorbance at 652 was used to back calculation of the concentration of oxidized product by Lambert-beer law with the help of molar extinction coefficient (39000 $M^{-1}C^{-1}$ for ox-TMB) as shown in **equation 3.1.**

$$C = A/\text{Ɛ}b \qquad \textbf{3.1}$$

Where C is the substrate concentration, A is the absorbance of the medium, b is the thickness of the solution and Ɛ is the molar extinction co-efficient.

The steady-state for the rate of reaction was obtained from the slope of absorption change with time. In the typical experiment varies the H_2O_2 concentration (0.1 to 1 mmol/L) at the fixed TMB concentration (0.8 mmol/L) and their UV-visible absorbance spectra were traced by time course mode (**Figure 3.13a**). In the similar way varies the concentration of TMB (0.2 to 1.2 mmol/L) at fixed concentration of H_2O_2 (0.5 mmol/L) (**Figure 3.13d**). The double reciprocal graph obtained from the initial velocity by keeping one substrate constant (H_2O_2) and changing the other (TMB) and vice-versa, which proved catalytic behavior of N-CQDs (**Figure 3.13c and f**). The obtained plot showed the parallel line indicated the ping-pong mechanism. This result confirmed that at the time of reaction N-CQDs bound and reacted to one substrate and loose the primary product before bounding second substrate [Singh *et al* (2018)].The Lineweaver-Burk plot (**Figure 3.13b,e**), Michaelis–Menten constant (K_m) and maximum velocity (V_{max}) were obtained from Michaelis-Menten kinetic **equation 3.2**.

$$\frac{1}{v} = \frac{K_m}{V_{max}}\frac{1}{[S]} + \frac{1}{V_{max}} \qquad \textbf{3.2}$$

Where, v is the initial velocity of reaction, K_m is the Michaelis-Menten constant, V_{max} is the maximum velocity of reaction and [S] is the concentration of the substrate. The smaller K_m value leads to the stronger affinity amid the enzyme and substrate.

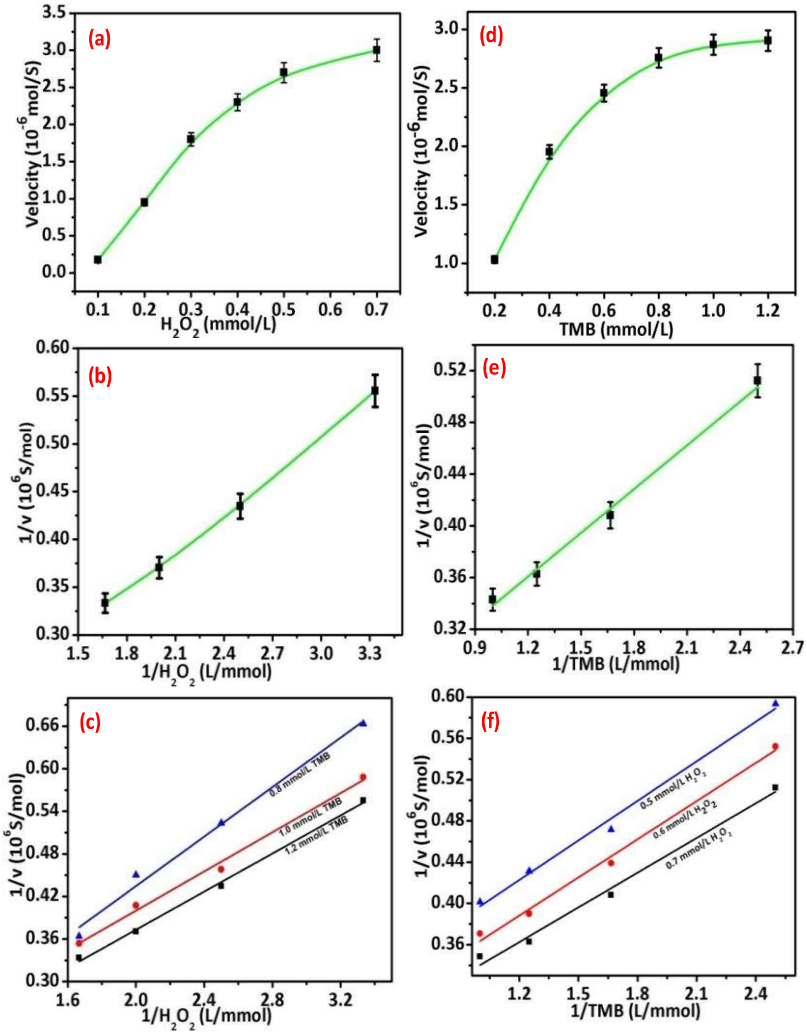

Figure 3.13 Represents the steady-state reaction rate and catalytic mechanism of the N-CQDs. (a and d) represent the michaelis-Menten curve at fixed TMB varying H_2O_2 concentration (a) and at fixed H_2O_2 varying TMB concentration (d), (b and e) corresponding Lineweaver–Burk plots by varying H_2O_2, fixed TMB (b) and varying TMB, fixed H_2O_2 (e), (c and f) Double-reciprocal plots of N-CQDs at fixed TMB varying H_2O_2 concentration (c) at fixed H_2O_2, varying TMB concentration (f).

From the **Table 3.2**, it was observed that when H_2O_2 was the substrate, the Km value of the N-CQDs was lower as compare to the horseradish peroxidase (HRP) indicated that N-CQDs exhibited greater empathy towards H_2O_2 whereas on considering the TMB as substrate, the Km was analogous to the HRP indicating less empathy of N-CQDs for TMB as the substrate [Hang *et.al*. (2014)]. The higher affinity of N-CQDs towards H_2O_2 as the substrate was also supported by the previously published literature based on carbon dots [Chai *et.al.* (2015), Wang *et.al*. (2011), Zeng *et.al*. (2017), An *et.al*. (2013), singh *et.al*. (2018)].

Table 3.2

	K_m [mmol/L]		V_{max} [10^{-6} mol/S]		
Catalysts	H_2O_2	TMB	H_2O_2	TMB	Reference
HRP	3.702	0.434	8.71	10	Hang (2014)
BiW_9Cu_3	0.29	0.36	0.69	1.43	Chai (2015)
V_2O_5 nanoplates	0.058	0.165	1.4	2.4	Qu(2014)
CNPs	0.05	26.06	4.27	6.05	Wang (2011)
Carbon nanomaterials	0.01	2.45	10.31	155.9	Zeng (2017}
Fe_3O_4@C	0.072	0.38	17.99	73.99	An (2013)
N-CQDs	0.4913	0.515	4.38	4.49	**Present work**

Table 3.2 The Michalies-Menten constant (K_m) and maximum velocity (V_{max}) obtained from the Lineweaver-Burk plots of N-CQDs and comparable with HRP and others enzyme mimetic nanomaterials.

3.5. Mechanism of catalytic activity

To gain deeper insight into the mechanism of the peroxidase-like catalytic activity of N-CQDs, active species trapping experiment was conducted. The hydroxyl radical ($OH^{\cdot}$) scavenger such as isopropyl alcohol (IPA) and methyl alcohol (MA) was added to the reaction medium and UV-visible absorption spectra were performed. From the **Figure 3.14**, which showed that in the presence of IPA (red line) and MA (blue line) the absorption at 652 nm was decreased, i.e. incomplete oxidation of TMB due to consumption of $^{\cdot}OH$ radical by the IPA and MA. However, in the absence of $OH^{\cdot}$ scavenger (black line), maximum absorption occurred at 652 nm indicated the complete oxidation of TMB. This observation indicated that the strong oxidizing $^{\cdot}OH$ radicals generated in the peroxidase-like catalytic reaction in the presence of N-CQDs played a key role in oxidizing TMB to produce a blue color.

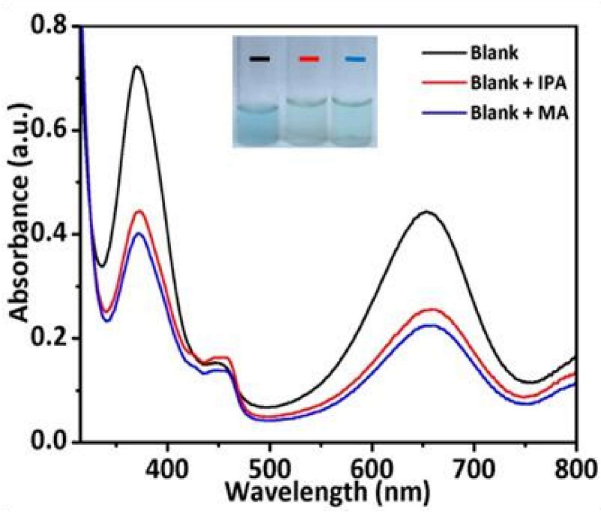

Figure 3.14 Absorbance spectra of ox-TMB in the absence and presence of different hydroxyl radical scavengers (IPA and MA) in the reaction system of TMB+H_2O_2+N-CQDs.

In Addition to this, the catalytic activity would be arisen due to small size, high surface area and abundance of negative charge density on the surface of N-CQDs. It was believed that

during oxidation process, the positively charged TMB molecule could be absorbed on to the surface of N-CQDs as chromogenic electron donors, and then TMB would transfer the lone-pair electrons from amino groups to the surface of N-CQDs, which results in an accumulation of electron density and mobility in N-CQDs. This would accelerate the electron transfer from N-CQDs to H_2O_2, resulting in the reduction of H_2O_2 to produce H_2O and ·OH radical. This ·OH radical oxidized the TMB via one electron transfer to produced blue color solution (**scheme 3.2**) [Lin *et.al*. (2014)].

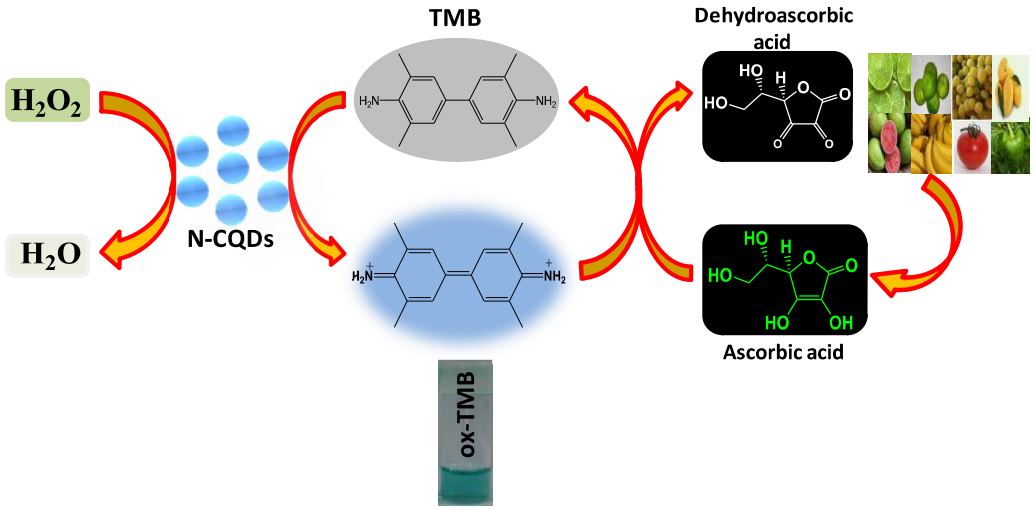

Scheme 3.2 Schematic representation of oxidation of TMB and colorimetric detection of AA in the real sample.

3.6. Detection of H_2O_2

The prospective application of Hydrogen peroxide (H_2O_2) in various field such as paper and pulp industry, cleaning and disinfecting agents, medicine, antibacterial agent and propellants in rockets made it an important molecule [Wolfbeis *et.al*. (2002)]. Addition to this, the biological

and enzyme-catalyzed reactions produced H_2O_2 as by-product which accumulated inside the cells causes inflammation due to the oxidative damage or modification of base pairs in DNA [Miller *et.al.* (2005)]. Hence, the accurate and trace level detection of H_2O_2 has always received much attention in the research community. Since the catalytic activity of N-CQDs towards the oxidation of TMB was H_2O_2 concentration dependent. Therefore, it provided an efficient tool for colorimetric detection of H_2O_2. To verify the detection ability, different concentration of H_2O_2 (0.02 to 2 mmol/L) was added to the reaction medium (30 µL N-CQDs + 40 µL TMB + 35µL H_2O_2 in 1 mL NaAc buffer (0.2 M at pH 4) and incubated for 10 min at RT, after that absorption spectra were recorded. It can be seen (**Figure 3.15a)** that as the concentration of H_2O_2 increases, absorption at 652 nm increases along with the color change from colorless to blue (**Inset Figure 3.15a**); indicated that the oxidation of TMB were proportional to the H_2O_2 concentrations. The detection system showed good linearity in the concentration range 0.1 to 0.5 with a correlation coefficient (R^2 = 0.998) (**Inset Figure 3.15b**) and the calculated LOD was 0.035 mmol/L which was better than those of previously reported literatures [Liu *et.al.* (2012), Yung *et.al.* (2016)].

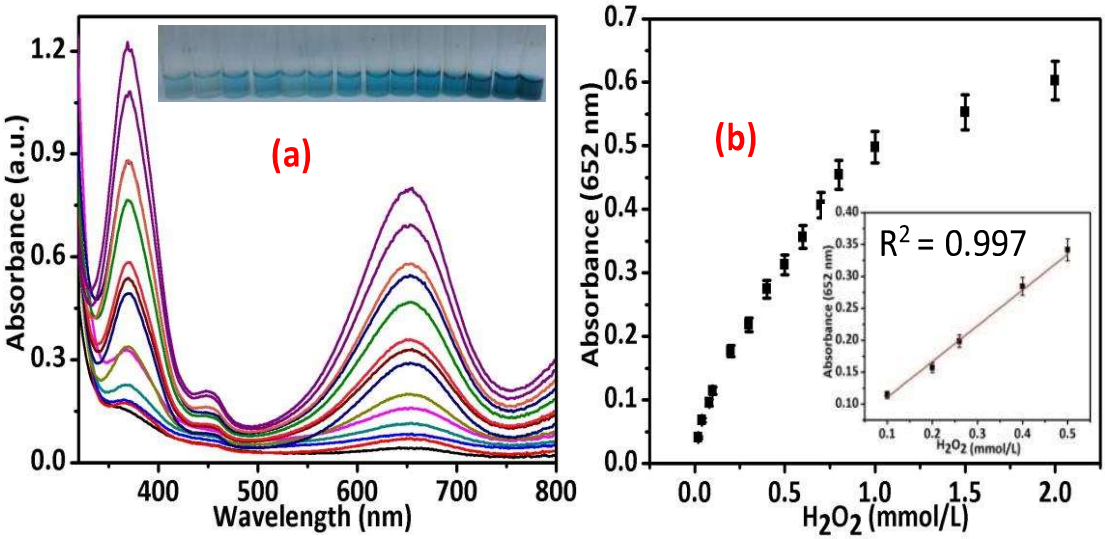

Figure 3.15. (a) Shows the absorbance spectra of ox-TMB on varying the concentration of H_2O_2 from 0.02 to 2 mmol/L with color change of (inset), (b) absorbance at 652 nm and its linear calibration plot in a range 0.1-0.5 mmol/L for the H_2O_2 detection based on peroxidase-like oxidation of TMB.

3.7. Detection of Ascorbic acid

The blue color of ox-TMB provides an outstanding platform towards the detection of reductant molecules. To investigate the reduction of ox-TMB, UV-visible sensitivity experiment was conducted by adding up the different concentration of AA (0-120 µM) in ox-TMB. From **Figure 3.16a,** as the concentration of AA increases, the absorption maxima were decreased at 652 nm with the color change to transparent from blue (**inset Figure 3.16 a**). This concluded that the reduction of ox-TMB was proportional to the AA concentration. The AA dependent reduction of ox-TMB showed the good linearity in the range 5 to 40 µM AA concentration with a linear correlation $R^2 = 0.998$ (**inset Figure 3.16 b**). The calculated LOD was 1.773 µM, better than the earlier reported literatures (**Table 3.3**) [Abbasi *et.al*. (2018), Sun *et.al*. (2012), Mi *et.al*. (2013), Weng *et.al*. (2011), Ai *et.al*. (2013), Wang *et.al*. (2002).

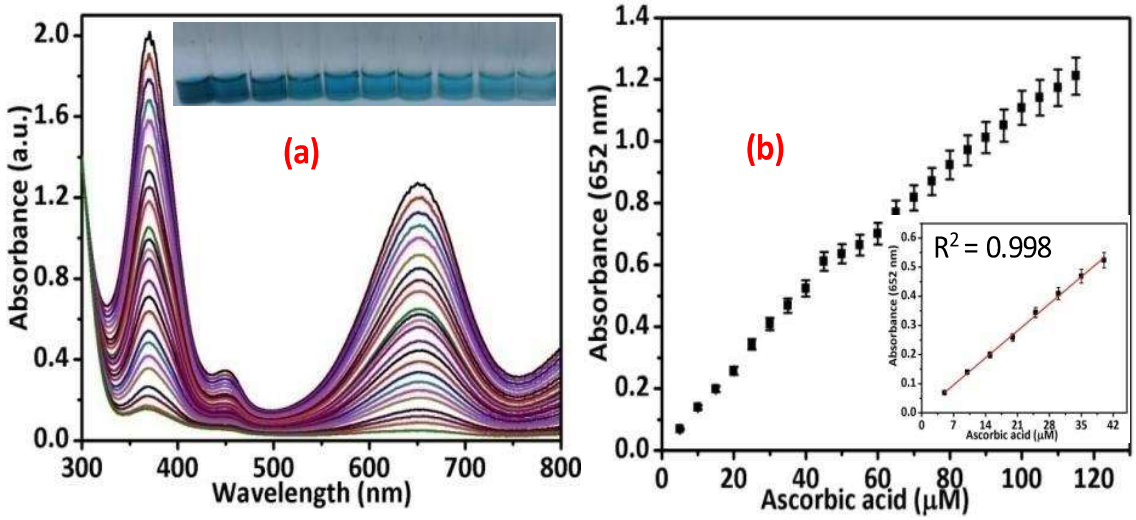

Figure 3.16 (a) Absorbance spectra of ox-TMB on varying the AA concentrations from 0 to 120 µM with change of color (inset photograph), (b) Absorbance at 652 nm and linear calibration plot ranges between 5-40 µM for the AA detection.

Table 3.3

Probe	Linearity range (µM)	LOD (µM)	Reference
N,S-CDs	10-200	4.69	34
Schiff base	10-390	2.4	63
SnO_2	100-5000	50	64
LaF_3:Ce,Tb	8-10	2.4	65
EPS	0-1000	7.35	66
MOF-808	30-1030	15	16
MIL-53(Fe)	28.6-190.5	15	67
CNT	80-136	20	68
N-CQDs	5-40	1.773	**Present work**

Table 3.3 The comparison of earlier reported literatures with the proposed method for the AA detection.

Since, the sensing of AA and H_2O_2 depends on peroxidase-mimetic catalytic action of N-CQDs by oxidoreduction of TMB which were entirely color dependence. **Figure 3.17** showed that fluorescence emission intensity of N-CQDs was slightly quench in the existence of TMB (N-CQDs + TMB), but in the existence of H_2O_2 (N-CQDs + TMB + H_2O_2), the emission intensity was entirely quenched showing the complete oxidation of TMB. However, in existence of ascorbic acid (N-CQDs + TMB + H_2O_2 + AA), the ox-TMB get reduced to TMB. As a result of this, the N-CQDs recover its fluorescent properties. On the basic of this observation, we can say that the as synthesized N-CQDs are reusable.

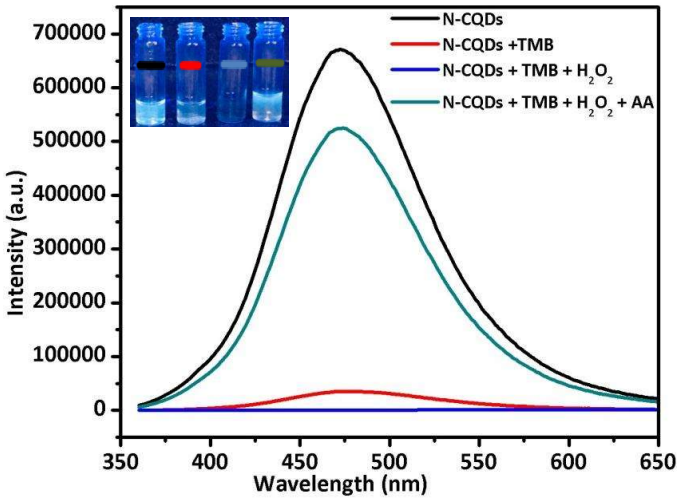

Figure 3.17 Fluorescence spectrums of N-CQDs in different system with inset photograph taken under UV-light.

The sensing system was highly influenced by interfering molecule and ions therefore to establish the selective and sensitive detection; interference test was carried out by UV-visible

absorption experiment. To investigated the test, different inorganic and organic reducing agents including KI, KBr, glucose, cinnamic acid, citric acid, benzoic acid, oxalic acid, adipic acid, tartaric acid, uric acid and dopamine were added into the ox-TMB solution. There were insignificant changes observed in the absorption maxima of ox-TMB in the presence of these reducing agents. However, in the presence of AA, the absorbance at 652 nm of ox-TMB s decreased with alteration of color (blue to transparent) indicated the selective detection of AA (**Figure 3.18**).

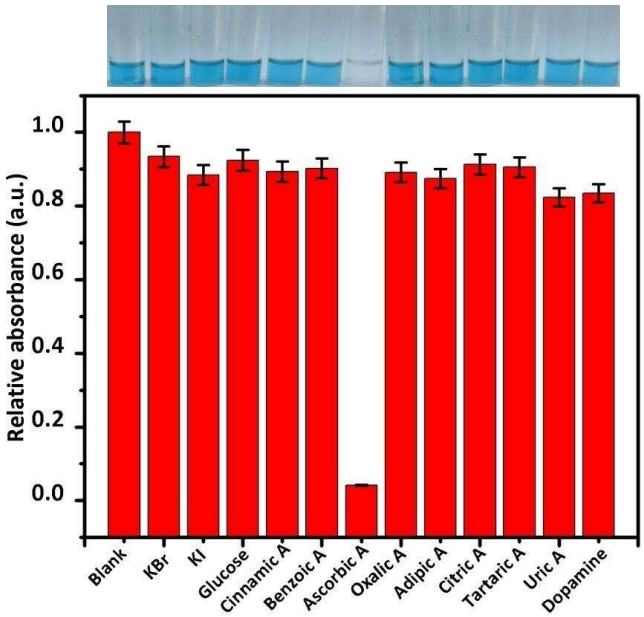

Figure 3.18. The interference of different reducing agents in the AA detection and upper photograph showed selective sensing of AA.

3.8. Sensing of AA in fresh fruits juice

The sensible practicability of AA detection was investigated in different fresh fruits such as tomato, mango, grapes, lemon, orange, papaya, bell pepper, and guava juices. In 1mL of ox-TMB blue color solution, 40 µL of each fruit juices were added and found maximum decrease in case of guava juice while least in presence of tomato juice, this observation indicated that the reduction ability of guava juice was better than tomato juice. The obtained result confirmed that the content of AA was maximum in the guava juice while minimum in tomato. This was further confirmed by color changed (blue to transparent) (**Figure 3.19**). Thus, sensing of ascorbic acid in real sample by ox-TMB advocated the practical application for routine detection of AA in the biological sample.

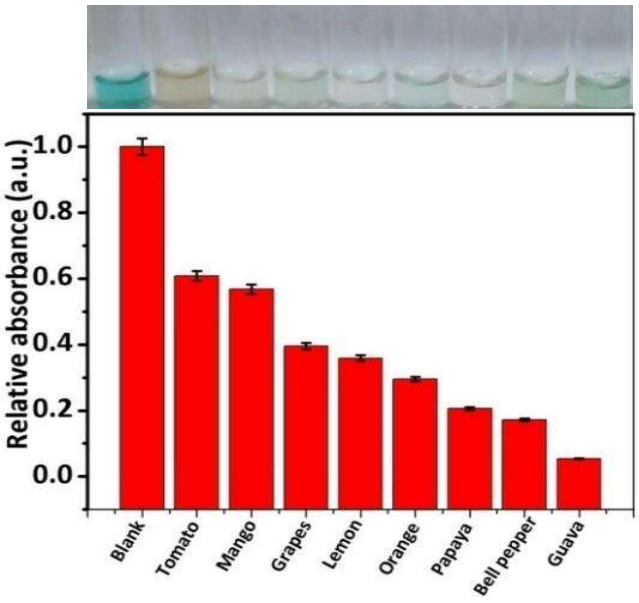

Figure 3.19 Showed the AA detection in different fruit samples whereas photograph of vial showing the corresponding color change.

Further, to examine some interference such as amino acids in fresh fruits for AA detection, an investigation was carried out and founded almost no effect on the absorbance of oxidized-TMB at 652 nm on adding different amino acids (**Figure 3.20**). It means that amino acid was not able to reduce the ox-TMB. This result strongly confirmed that AA present in the fresh fruits was responsible to reduced Ox-TMB into its native form.

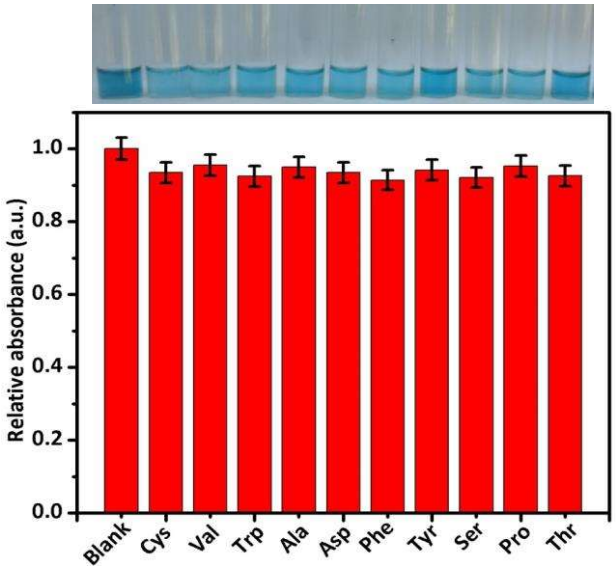

Figure 3.20 The interference of different amino acids for the AA detection in fresh fruits.

3.9. Conclusions

In brief, fluorescent N-CQDs have been successfully synthesized from *Azadirachta indica* leaves by using simple green one pot hydrothermal treatment. The synthesized N-CQDs showed the excitation-dependent fluorescence emission in a range 290-370 nm. The measured fluorescence QY of the N-CQDs was about 27.2 % by using quinine sulfate as a standard. The attractiveness

of the synthesized N-CQDs was that it exhibited peroxidase-like catalytic activity for the oxidation of peroxidase substrate TMB together with H_2O_2. After evaluation of kinetic properties, it was observed that it follow Michaelis-Menten kinetic activity and steady-state kinetic analysis reveals that the oxidation of TMB was based on ping-pong mechanism. Addition to this, the LOD for H_2O_2 detection was 0.035 mmol/L in a linear range between 0.1-0.5 mmol/L. The ox-TMB acted as a probe for the AA detection with the good selectivity and the measured LOD was found to be 1.773 µM in a linear range of 5-40 µM. Addition to this, the ox-TMB based sensing system was further applied for detection of AA in the real sample such as different varieties of common fruits which showed the detection ability accordingly the amount of the AA content in the fruits. Therefore, the applied sensing system advocated the excellent feasibility for the routine analysis of AA in the biological sample.